University of Birmingham

Investigation of PO_4^{3-} oxyanion-doping on the properties of $CaFe_{0.4}Ti_{0.6}O_{3-\delta}$ for potential application as symmetrical electrodes for SOFCs

dos Santos-Gómez, Lucía ; Porras-Vázquez, Jose; Losilla, Enrique; Marrero-López, David; Slater, Peter

[Link to publication on Research at Birmingham portal](#)

Investigation of PO_4^{3-} oxyanion-doping on the properties of $CaFe_{0.4}Ti_{0.6}O_{3-\delta}$ for potential application as symmetrical electrodes for SOFCs.

Lucía dos Santos-Gómez[1,2*], José M. Porras-Vázquez[2,*], Enrique R. Losilla[2], David Marrero-López[3], Peter R. Slater[4]

[1] Department of Physical and Analytical Chemistry, Oviedo University-CINN, 33006-Oviedo, Spain.

[2] Universidad de Málaga, Dpto. de Química Inorgánica, Cristalografía y Mineralogía, 29071-Málaga, Spain.

[3] Universidad de Málaga, Dpto. de Física Aplicada I, 29071-Málaga, Spain.

[4] School of Chemistry, University of Birmingham, Birmingham, B15 2TT, United Kingdom.

Abstract

$CaTi_{0.6-x}Fe_{0.4}P_xO_{3-\delta}$ ($0 \leq x \leq 0.075$) perovskite series are investigated as potential symmetrical electrodes for SOFCs. Pure phase compounds with a cubic perovskite structure (s.g. $Pm\bar{3}m$) are obtained for $x \leq 0.025$, while higher doping level leads to the formation of $Ca_{10}(PO_4)_6(OH)_2$ as secondary phase. The P-doped compounds are structurally stable under reducing atmosphere unlike the undoped phase. Conductivity values of the P-doped samples are slightly higher than that of the undoped one, i.e. 0.11 and 0.07 Scm^{-1} for $CaTi_{0.575}Fe_{0.4}P_{0.025}O_{3-\delta}$ and $CaTi_{0.6}Fe_{0.4}O_{3-\delta}$, respectively, at 750 ºC in air. The performance of $CaTi_{0.575}Fe_{0.4}P_{0.025}O_{3-\delta}$ acting simultaneously as both anode and cathode was also tested in a symmetrical solid oxide fuel cell with a 240 µm thick YSZ electrolyte. Hence, these results show that PO_4^{3-} units can be introduced into $CaTi_{0.6}Fe_{0.4}O_{3-\delta}$ perovskite structure, having beneficial effects on the electrochemical performance and the phase stability.

* Corresponding author.
E-mail address: ldsg@uniovi.es (Lucía dos Santos-Gómez)
Present address: Department of Physical and Analytical Chemistry, Avda. Julián Claveria 8, Campus de El Cristo, Oviedo University-CINN, 33006-Oviedo, Spain.
Tel: +34 605975563

1. Introduction

A typical Solid Oxide Fuel Cell (SOFC) device is comprised of three specific ceramic elements: cathode, electrolyte and anode, all of them with different and well-defined compositions. This heterogeneity leads to numerous fabrication steps during the assembly of the device, with the concomitant losses of energy, money and time, as well as the possibility of not desired reactivity between the cell components during the manufacturing processes.

All these disadvantages could be solved with a new SOFC configuration, symmetrical solid oxide fuel cells (SSOFCs), where cathode and anode are composed by the same material with good stability and adequate electrochemical properties in both oxidising and reducing conditions [1-5]. This approach largely simplifies the fabrication process, since both electrodes are deposited and sintered in only one thermal treatment. This cell configuration also results in lower fabrication costs and improved chemical and mechanical stability of the device since the same type of interfaces are presented on both sides of such cell.

Diverse families of materials have been tested as promising electrodes for SSOFCs, such as $Pr_2NiO_{4\pm\delta}$, $Nd_2MnO_{4\pm\delta}$ and $La_{0.5}Sr_{1.5}MnO_{4\pm\delta}$ systems with the Ruddlesden-Popper structure; $La_2CoTi_{0.7}Mg_{0.3}O_{6-\delta}$ and $Sr_2Fe_{1.5}Mo_{0.5}O_{6-\delta}$ double perovskites; and $PrNi_{0.4}Fe_{0.6}O_{3-\delta}$, $La_{0.75}Sr_{0.25}Cr_{0.5}Mn_{0.5}O_{3-\delta}$, $La(Fe,Ni)O_{3-\delta}$, $SrFeO_{3-\delta}$ and $SrCoO_{3-\delta}$ simple perovskites, which is the system more extensively studied for these type of applications [5-17]. Most of these electrodes contain easily reducible transition metals, such as Co, Cu and Ni, and therefore these electrodes suffer a phase transformation under reducing atmospheres, which possibly leads to mechanical failure of the cells due to volume changes upon redox cycles. For this reason, it is essential to find new materials to work as symmetrical electrodes with a stable structure in both oxidizing and reducing atmospheres.

In this sense, $ATiO_3$ (A=Ca, Sr, Ba) perovskites with partial replacement of titanium by iron have been hugely studied due to the significant interest of creating mixed ionic and electronic conductivity when these perovskites are doped with different multivalent cations [18]. The structure of iron-substituted calcium titanates was firstly characterized by Grenier *et al.* using X-ray diffraction, transmission electron microscopy and Mössbauer spectroscopy studies [19,20]. The $CaTi_{1-y}Fe_yO_{3-\delta}$ system is described as an intermediate material between two structures, the $CaTiO_3$ perovskite and the $Ca_2Fe_2O_5$ brownmillerite. The importance of such compounds lies in their ability to accommodate anion vacancies and therefore support the electrical neutrality when Ti^{4+} is interchanged by Fe^{3+} [18,21-29]. The electronic and ionic conductivity of $CaTi_{1-y}Fe_yO_{3-\delta}$ depend on the oxygen vacancy concentration and the degree of ordering of the oxygen sublattice, which determines their mobility. Oxygen vacancies are randomly allocated for samples with y<0.5,

however, long-range ordering occurs when y≥0.5 [30]. Such ordering of the oxygen vacancies is detrimental for practical implementations, since it seriously reduces the ion conduction and also decreases the concentration and mobility of hole carriers [30]. In this context, $CaTi_{0.6}Fe_{0.4}O_{3-\delta}$ is the composition with the highest Fe-content and disordered oxygen vacancies, making it a potential candidate for symmetrical SOFCs. Moreover, the materials under study in this work are reported to exhibit high stability in H_2 and CO_2 atmospheres, they are cheaper compared to the above mentioned symmetrical electrodes and exhibit thermal expansion coefficient compatible with the conventional electrolytes [47].

Recently, the properties of simple perovskites (ABO_3) have been modified by the incorporation of oxyanions, such as BO_4^{5-}, SiO_4^{4-} and PO_4^{3-}, into the ionic framework [31-34]. Under this approach, the octahedral BO_6 unit is replaced by a tetrahedral oxyanion, and therefore, generating two oxide vacancies that favours the ionic conductivity. Moreover, in order to maintain the lattice electroneutrality, the B^{n+} species are reduced to $B^{(n-1)+}$, creating an effect of electron doping, which enhances the electronic conductivity. Hence, oxyanion doping is a promising strategy to improve the properties of the materials for the hydrogen oxidation reaction (HOR) and the oxygen reduction reaction (ORR). This approach has been successfully applied to different systems, such as $CaMnO_{3-\delta}$, $Ba_{0.5}Sr_{0.5}Co_{0.8}Fe_{0.2}O_{3-\delta}$ and $SrFeO_{3-\delta}$, where oxyanion doping leads to an enhancement of the electrical properties as well as the stabilization of high symmetric phases [35-37]. Recent works have extended the applications of such phosphate doped perovskites to low temperature oxygen evolution reaction (OER) and ORR catalysts [38-40].

The aim of this work is to explore the effect of the incorporation of PO_4^{3-} units into the framework of $CaTi_{0.6}Fe_{0.4}O_{3-\delta}$ perovskite in order to obtain a stable material with higher ionic conductivity than the undoped one, and examine its influence on the structural and the electrochemical properties with the goal of its potential application as electrodes for SSOFCs.

2. Experimental

2.1. Synthesis

Materials with composition $CaTi_{0.6-x}Fe_{0.4}P_xO_{3-\delta}$ (x = 0, 0.025, 0.05 and 0.075) were prepared by using the freeze-drying method and the same synthetic procedure detailed in previous works for comparable materials [41]. Stoichiometric solutions of $CaCO_3$ (99%, Alfa Aesar), $Ti[OCH(CH_3)_2]_4$ (99%, Aldrich), $Fe(NO_3)_3 \cdot 9H_2O$ (99.95%, Aldrich) and $(NH_4)_2HPO_4$ (99%, Aldrich) were elaborated by dissolving in different beakers $CaCO_3$ in diluted nitric acid, $Ti[OCH(CH_3)_2]_4$ in absolute ethanol, and $Fe(NO_3)_3 \cdot 9H_2O$ and $(NH_4)_2HPO_4$ in distilled water. An ethylenediaminetetraacetic acid solution

(99.99%, Aldrich) was incorporated as a complexing agent into the different metallic salts in a molar ratio 1:1. After that, all cation solutions were combined, getting a transparent solution with concentration of 0.1 mol L^{-1} and pH~8. Precursor solutions were slowly dripped and frozen into liquid N_2 and then dehydrated in a Scanvac Coolsafe freeze-dryer for 48 hours, obtaining dried powders which were calcined at 300 and 800 ºC for 1 h to remove the organic material and the remaining carbonaceus species, respectively.

The resulting powders were compacted into cylindrical disks of 10 and 1 mm of diameter and thickness, respectively, and sintered at 1200 and 1400 ºC for P-doped and undoped samples, respectively, for 4 h with heating/cooling rates of 5 ºC min^{-1}. Hereafter, $CaTi_{0.6-x}Fe_{0.4}P_xO_{3-\delta}$ samples are labelled as P_x where x is the phosphorus content.

2.2. Structural, microstructural and thermal characterization

Laboratory X-ray powder diffraction (XRPD) was employed to analyze the composition and structure of all the compounds. The diffractometer used was a PANalytical X´Pert Pro MPD equipped with a X´Celerator detector and $CuK_{\alpha 1}$ radiation. The phase identification and structural analysis were performed using the X'Pert HighScore Plus and GSAS softwares [42,43].

The morphology and composition of the pellets were examined by field emission scanning electron microscopy (FEI-SEM, Helios Nanolab 650) and energy-dispersive X-ray spectroscopy (EDX, Oxford Instruments). The grain size was estimated by the linear intercept method [44].

The phase stability in reducing atmosphere was investigated by exposing the powder to a regular 5%H_2-Ar flow at 800 ºC for 2 days.

For the chemical compatibility studies, the $CaTi_{0.575}Fe_{0.4}P_{0.025}O_{3-\delta}$ sample and commercial electrolyte powder, $Zr_{0.84}Y_{0.16}O_{1.92}$ (YSZ, Tosoh), were mixed in a 50 wt.% and annealed in air at different temperatures for 1 day. The resulting mixtures were analyzed by XRPD.

The Oxygen stoichiometry was calculated by thermogravimetric analysis (Mettler Toledo) from 30 to 1200 ºC under a 50 mL min^{-1} N_2 flow and a heating/cooling rate of 10 ºC min^{-1}.

2.3. Electrical characterization

Impedance spectra were obtained by using a Solartron 1260 FRA in two different atmospheres: air (for cathode applications) and 5%H_2-Ar (for anode applications). The data were acquired in intervals of 50 ºC from 800 down to 150 °C with an ac perturbation and a stabilization time between successive measurements of 100 mV and 45 min, respectively. Pt-ink (METALOR® 6082) was deposited on the both sides of the pellet surfaces, and a heating treatment at 800 ºC for 15 min was carried out to sinter the Pt current collectors.

Area specific resistance (ASR) values were acquired in both oxidizing and reducing atmosphere, air and 5%H_2/Ar. Electrodes were prepared by mixing the powders with Decoflux^{TM} (Zschimmer & Schwarz) to obtain a slurry that was used to symmetrically paint on dense pellet of YSZ electrolyte. Symmetrical cells were annealed at 1000 ºC for 1 h to ensure an adequate adhesion. Pt ink was applied onto both electrodes and fired at 800 ºC for 15 min to obtain a current collector. The stability and reversibility of electrodes were evaluated by switching the O_2 and H_2 gases.

2.4. Fuel cell performance

Electrolyte supported cells were prepared to investigate the electrochemical performance of the P-doped samples in SOFC conditions. The electrolyte was prepared by compacting commercial YSZ powders (Tosoh) into a disk of 13 and 0.25 mm in diameter and thickness, respectively, following by sintering at 1400 ºC for 4 h. An ink was prepared from the P-doped powders and Decoflux^{TM} (Zschimmer & Schwarz) and was symmetrically screen-printed on both faces of the YSZ pellet, which was finally sintered at 1000 ºC for 1 h. The area where the symmetrical electrodes were deposited was restricted to 0.25 cm^2. A ceramic paste (Ceramabond 668, Aremco) was employed to seal the symmetrical cell on an alumina device. The impedance and current-voltage plots were acquired using a Bio-Logic VSP potentiostat/galvanostat/FRA in the 650-800 ºC temperature range. Static air and H_2 were employed as oxidant and fuel, respectively.

3. Results and discussion

3.1. Single phase existence range and phase stability under reducing conditions

The undoped sample is a single phase with cubic type structure after sintering at 1400 ºC, in accordance with Becerro *et al.* [45]. At lower temperatures impurities of $Ca_2Fe_2O_{5+\delta}$ are detected (Figure 1a). In contrast, the introduction of a small amount of PO_4^{3-} units into the perovskite structure leads to a reduction of the synthesis-sintering temperature to 1200 ºC (Figure 1b).

XRPD patterns for the $CaTi_{0.6-x}Fe_{0.4}P_xO_{3-\delta}$ series (x = 0, 0.025, 0.05 and 0.075) are shown in Figure 2a. The compounds with P content x≤0.025 are single phase materials, higher dopant content leads to an increasing segregation of $Ca_{10}(PO_4)_6(OH)_2$ with an apatite-type structure (PDF number 96-901-3628) as a secondary phase (Table 1); however, despite this segregation, the whole series crystallize with a cubic perovskite-type structure.

XRPD data were analyzed by using the Rietveld method and a cubic perovskite-type structural model, with a $Pm\bar{3}m$ space group, was employed for all the refinements. Occupancy factors were fixed to the nominal stoichiometry, where Ti, Fe and P were located in the same

crystallographic position, and their isotropic atomic displacement parameters constrained to be the same. Parameters such as unit cell, scale factor, background, peak shape and isotropic displacement were refined. All samples were satisfactorily refined, obtaining favourable agreement factors (Table 1). An example of these fits is shown for $P_{0.025}$ in Figure S1. It has to be mentioned that the agreement factors were slightly worse for the undoped composition, P_0, in comparison with the P-doped samples, likely due to a small orthorhombic distortion that disappeared after doping due to the stabilizing effect of phosphorus.

The evolution of the unit cell volumes with the P content is shown in Table 1. In these series, a decrease of the unit cell volume is detected as the P content increases up to x=0.075. It is important to bear in mind for oxyanion-doped samples that the evolution of the cell parameters is a balance between two factors: (i) the smaller size of the tetrahedral PO_4 units in comparison to that of the octahedral TiO_6, which would lead to a decrease of the cell volume; and (ii) the replacement of the TiO_6 unit by the PO_4 one leads to the loss of two oxygens and the concomitant reduction of Fe^{4+} (0.585 Å) to Fe^{3+} (0.645 Å) in order to maintain the lattice electroneutrality, which results in an increase of the cell volume, according to the following equation:

$$(NH_4)_2HPO_4 + 4Fe_{Fe}^X + O_O^X \rightarrow P_{Fe}^{\cdot} + 3Fe_{Fe}' + V_O^{\cdot\cdot} + 2NH_3 + 3/2H_2O + 3/4O_2 + \text{``}FeO_2\text{''} \quad \textbf{Eq.1}$$
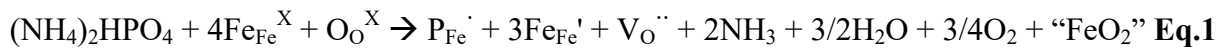
It has to be mentioned that "FeO_2" does not mean free iron oxide but Fe^{4+} that maintains its oxidation state after the oxyanion doping [37].

As can be seen in Table 1, for the whole $CaTi_{0.6-x}Fe_{0.4}P_xO_{3-\delta}$ series, the small size of phosphorus tetrahedral outweighs the iron reduction, for $0 \leq x \leq 0.075$, indicating that despite the segregation of $Ca_{10}(PO_4)_6(OH)_2$, part of the phosphorus is being still incorporated into the structure, leading to a decrease of the cell volume.

Structural stability in reducing conditions is a key factor in order to use these materials as symmetrical electrodes in SSOFCs. Partial decomposition or structural changes of the electrode phases might produce volume alterations during the reduction and oxidation cycles, causing delamination in the cell. Thus, in order to ensure the reliability of these P-doped compounds under reducing conditions, stability tests were conducted. In Figure 2b it can be seen that the undoped composition, P_0, is unstable under such reducing conditions, leading to a variation in symmetry, from a cubic to an orthorhombic phase. This modification is due to the partial reduction of Fe to lower oxidation states, which causes oxygen losses in the structure and modification of the oxygen sublattice. An opposite behaviour is observed for the P-doped samples, which are stable under the same reducing conditions and maintain the cubic symmetry, including those with $Ca_{10}(PO_4)_6(OH)_2$ as secondary phase. In addition, the cell parameters for the whole series increase after the thermal treatment in reducing conditions, due to the change from Fe^{4+} to Fe^{3+} (Table 1). Therefore, these

results highlight the beneficial effect of the incorporation of phosphorus into the structure, leading to an enhancement in the redox stability and its possible use as symmetrical electrode for SOFCs.

All samples were also analyzed by thermogravimetric analysis to determine the oxygen stoichiometry, following a comparable process described in the literature [36,37]. The mass losses of the samples are utilized to calculate the average oxidation state of the iron cations and the oxygen stoichiometry. As can be appreciated in Figure 3, both the oxygen deficiency (δ) and the average oxidation state of iron cations decrease with the P-content, i.e. oxidation states of 3.110 and 3.042 for P_0 and $P_{0.075}$, respectively. These results confirm that most of the iron is present as Fe^{3+}, as expected, although a small contribution of Fe^{4+} is possibly presented, in accordance with previous Mössbauer spectroscopy studies for related compounds [46]. The amount of Fe^{3+} increases with the P content because the introduction of PO_4^{3-} leads to the reduction of Fe^{4+} to Fe^{3+} to maintain the lattice electroneutrality (Eq. 1).

3.2. Microstructural characterization

Figure 4 shows the superficial SEM images of the $P_{0.025}$, $P_{0.05}$ and $P_{0.075}$ samples sintered at 1200 ºC for 4 h. These images reveal that the ceramic pellets are well sintered with densities higher than 96%. Analysis of the P-doped samples indicates that the incorporation of phosphorus into the structure does not change significantly the microstructure of the materials, with an average grain size of 2 μm (Figure 4a-c). However, $P_{0.075}$ exhibits slightly smaller grain ~1 μm, possibly due to the presence of larger amounts of secondary phases.

EDX mapping for $P_{0.025}$ reveals that there is a good bulk distribution for all the elements and phase segregations at the grain boundaries are not detected (Figure 4d). However, for x≥0.05, P-enriched grains are observed, ascribed to the $Ca_{10}(PO_4)_6(OH)_2$ segregation, which increases with the P-content (Figure 4e and f). These results confirm the extremely low solubility of phosphorus in the $CaTi_{0.6}Fe_{0.4}O_{3-\delta}$ structure, which is in agreement with the XRPD data.

3.3. Electrode-electrolyte compatibility

The reactivity between the electrolyte and electrodes is an important aspect to be considered during the fabrication of a SOFC because an excessive sintering temperature could lead to the formation of interfacial phases, which possibly block the oxide ion transport and increase the ohmic resistance of cell. Thus, taking into consideration that the minimum temperature required to obtain an optimal adherence of these P-doped materials with YSZ electrolyte is 1000 ºC, the chemical compatibility study was carried out up to this temperature. Figure 5 shows the XRPD patterns of the mixtures of $P_{0.025}$ electrode with YSZ electrolyte at different temperatures for 24 h. Neither appreciable undesired phases nor variation in the cell parameters were observed, indicating that these

compounds are chemically compatible to be used simultaneously in a cell in the temperature range studied between 800 and 1000 °C.

On the other hand, the thermal compatibility of the electrodes with the electrolyte material is crucial for practical application. $CaTi_{0.6}Fe_{0.4}O_{3-\delta}$ provides a reasonable thermal expansion coefficient (TEC) with regard to the most commonly used electrolyte, YSZ, as has been reported by Kharton *et al.*, i.e. 12×10^{-6} and 11×10^{-6} K^{-1} for P_0 and YSZ, respectively [47]. TEC values were not determined for the P-doped compounds; however, a small amount of P-doping is not expected to affect significantly the TECs, since the lattice oxygen stoichiometry and average oxidation states of iron are slightly affected as discussed above.

3.4. Electrical characterization

According to the literature data, the conductivity of $CaTi_{1-y}Fe_yO_{3-\delta}$ series is very sensitive to the temperature and the oxygen stoichiometry [28]. Moreover, the oxyanion doping has a large influence on the electronic and ionic conductivity of similar perovskite structure materials [3,36]. The conductivity of these series was measured in two different atmospheres: air and 5%H_2-Ar. For all samples, the conductivity variation with the temperature shows a semiconductor-type behaviour in the whole temperature range investigated. In oxidising conditions, the conductivity of the $CaTi_{0.6-x}Fe_{0.4}P_xO_{3-\delta}$ series increases up to x = 0.05, associated with the incorporation of phosphorus into the structure, which increases the oxygen vacancy concentration as demonstrated earlier by the defect equation (Eq. 1). Higher P-content leads to a decrease in conductivity possibly due the disrupting effect of phosphorus segregations.

In order to prove the beneficial effect of P-doping, and its incorporation into the structure, a phosphorus-free sample derived from $CaTi_{0.575}Fe_{0.4}P_{0.025}O_{3-\delta}$ was prepared, with formula $CaTi_{0.575}Fe_{0.4}O_{3-\delta}$ and cation deficient in the perovskite in B-site. As can be seen in Figure 6a, the conductivity of this sample decreases significantly with values even lower than those of the undoped composition. These results clearly confirm that the improvement of conductivity in P-doped samples is due to the replacement of octahedral TiO_6 units by tetrahedral PO_4 ones.

In reducing conditions the conductivity decreases for all compositions due to the almost complete reduction of Fe^{4+} to Fe^{3+}, resulting in a significant decrease of the charge carriers, which is mainly associated with electron-hopping (Figure 6b). However, the conductivity of the $P_{0.025}$ sample in reducing conditions is slightly higher than the undoped one, i.e. 0.11 and 0.07 Scm^{-1}, respectively, at 750 ºC, likely due to higher number of oxygen vacancies (Eq. 1) and the improved stability of the cubic phase on P-doping, whereas P_0 decomposes in reducing conditions.

Figure 6c compares the temperature dependence of the polarization resistance values (R_p) for the P_0 and $P_{0.025}$ compounds in air and 5%H_2-Ar atmospheres. $P_{0.025}$ sample shows slightly lower R_p values than the undoped sample in air, i.e. 0.30 and 0.38 Ωcm^2 at 800 ºC, respectively. In a 5%H_2-Ar atmosphere, the R_p values for $P_{0.025}$ are quite similar to those measured in air but the R_p differences between these two atmospheres are more pronounced at lower temperature, i.e. 100.28 and 70.43 Ωcm^2 at 600 ºC in air and 5%H_2-Ar, respectively, possibly due to the lower activation energy for HOR (1.68 eV) compared to ORR (1.95 eV), improving the HOR. The undoped sample was not measured in H_2 atmosphere due to the phase transformation of this compound in such conditions.

3.5. Fuel cell test

Fuel cell tests were carried out to prove that P-doped samples can operate simultaneously as both anode and cathode in SSOFC. Figure 7a shows the power density and the current-voltage curves for $P_{0.025}$/YSZ/$P_{0.025}$ electrolyte-supported cell at different temperatures. The open circuit voltage (OCV) matches well with the theoretical value expressed by the Nernst equation (~1.1 V). This cell generated a maximum power density of 58 $mWcm^{-2}$ at 800 ºC. This value is not extremely high due to the high ohmic resistance of the thick YSZ electrolyte. Similar performance values have been reported in the literature for similar SSOFCs with thick electrolytes, i.e. 50.7 $mWcm^{-2}$ at 800 ºC for $La_{0.7}Ca_{0.3}Cr_{0.97}O_{3-\delta}$/YSZ/$La_{0.7}Ca_{0.3}Cr_{0.97}O_{3-\delta}$ and 90 $mWcm^{-2}$ at 950 ºC for $La_{1.3}Sr_{2.3}(Ti_{1-x}Fe_x)O_{3\pm\delta}$/YSZ/$La_{1.3}Sr_{2.3}(Ti_{1-x}Fe_x)O_{3\pm\delta}$ [50,51]. P_0/YSZ/P_0 electrolyte-supported cell was not prepared since the undoped composition, P_0, is not stable under reducing conditions as previously discussed.

Figure 7b shows a cross-sectional image of this cell. The adhesion between the electrolyte and the symmetrical electrodes is quite good and an adequate porosity is observed after the electrical characterization, without appreciable delamination or reactivity at the electrode/electrolyte interface. The electrolyte is fully dense and has a thickness around 240 μm. Thus, the power density values could be considerably improved by decreasing the electrolyte thickness.

In summary, the results obtained in the present work suggest that P-doped $CaTi_{0.6}Fe_{0.4}O_{3-\delta}$ samples are alternative and promising symmetrical electrode materials for SOFCs. However, further investigation is necessary to improve the performance by optimizing the microstructure of the cell, i.e. by reducing the thickness of the electrolyte or alternatively by using nanostructured electrodes obtained by low deposition methods, such as spray-pyrolysis [48,49].

Conclusions

$CaTi_{0.6-x}Fe_{0.4}P_xO_{3-\delta}$ series (x = 0, 0.025, 0.05 and 0.075) have been prepared by the freeze-dried precursors method, obtaining single phase compounds for x≤0.025. The introduction of a small quantity of PO_4^{3-} units into the $CaTi_{0.6-x}Fe_{0.4}P_xO_{3-\delta}$ structure reduces the synthesis-sintering temperature from 1400 to 1200 ºC. The unit cell volumes decrease with increasing P-content without a significant change in the morphology of the materials. Phosphorus enriched zones, ascribed to $Ca_{10}(PO_4)_6(OH)_2$ segregations, were detected by EDX analysis for x≥0.05, confirming the extremely low solubility of the phosphate groups in the structure. Annealing experiments in $5\%H_2$-Ar showed improved redox stability for the P-doped compounds in contrast to the undoped one. Moreover, the conductivity values for P-doped samples are slightly higher than those of the undoped one in both oxidising and reducing atmospheres. Hence, these results show that phosphorus can be successfully incorporated into calcium iron titanate perovskites, having beneficial effects on the conductivity and phase stability in both oxidising and reducing conditions, making these compounds potentially suitable for symmetrical electrode applications. This work also shows the first results for the performance of a SOFC with symmetrical oxyanion-doped electrodes and suggest that further studies on related materials with optimized electrode microstructure are warranted. Furthermore, they may have other potential applications, given recent reports of phosphate doped perovskites as low temperature OER/ORR catalysts.

Acknowledgments

References

[1] J.C. Ruíz-Morales, J. Canales-Vázquez, J. Peña-Martínez, D. Marrero-López, P. Núñez, On the simultaneous use of $La_{0.75}Sr_{0.25}Cr_{0.5}Mn_{0.5}O_{3-\delta}$ as both anode and cathode material with improved microstructure in solid oxide fuel cells, Electrochim. Acta 52 (2006) 278-284.

[2] B. Wei, Z. Lü, X. Huang, M. Liu, N. Li, W. Su, Synthesis, electrical and electrochemical properties of $Ba_{0.5}Sr_{0.5}Zn_{0.2}Fe_{0.8}O_{3-\delta}$ perovskite oxide for IT-SOFC cathode, J. Power Sources 176 (2008) 1-8.

[3] J.C. Ruíz-Morales, D. Marrero-López, J. Canales-Vázquez, J.T.S. Irvine, Symmetric and reversible solid oxide fuel cells, RSC Advances 1 (2011) 1403-1414.

[4] C. Su, W. Wang, M. Liu, M.O. Tadé, Z. Shao, Progress and Prospects in Symmetrical Solid Oxide Fuel Cells with Two Identical Electrodes, Adv. Energy Mater. 5 (2015) 1500188.

[5] Y. Cao, Z. Zhu, Y. Zhao, W. Zhao, Z. Wei, T. Liu, Development of tungsten stabilized $SrFe_{0.8}W_{0.2}O_{3-\delta}$ material as novel symmetrical electrode for solid oxide fuel cells, J. Power Sources 455 (2020) 227951.

[6] L.A. Dunyushkinaland, V.A. Gorbunov, Crystal structure and electrical conductivity correlation in $CaTi_{1-x}Fe_xO_{3-\delta}$ system, Ionics 8 (2002) 256-261.

[7] A.J. Fernández-Ropero, J.M. Porras-Vázquez, A. Cabeza, P.R. Slater, D. Marrero-López, E.R. Losilla, High valence transition metal doped strontium ferrites for electrode materials in symmetrical SOFCs, J. Power Sources 249 (2014) 405-413.

[8] Z. Gao, X. Ding, D. Ding, L. Ding, S. Zhang, G. Yuan, Infiltrated Pr_2NiO_4 as promising bi-electrode for symmetrical solid oxide fuel cells, Int. J. Hydrog. Energy 43 (2018) 8953-8961.

[9] H. Tao, J. Xie, Y. Wu, S. Wang, Evaluation of $PrNi_{0.4}Fe_{0.6}O_{3-\delta}$ as a symmetrical SOFC electrode material, Int. J. Hydrog. Energy 43 (2018) 15423-15432.

[10] G.N. Mazo, N.V. Lyskov, S.Y. Istomin, E.V. Antipov, Evaluation of $La_2CoTi_{0.7}Mg_{0.3}O_6$ as an electrode material for a symmetrical SOFC, J. Electroceram. 40 (2018) 162-169.

[11] M.V. Sandoval, S. Durán, A. Prada, C. Pirovano, O. Gardoll, P. Roussel, G.H. Gauthier, Synthesis and preliminary study of $Nd_xAE_{2-x}MnO_{4\pm\delta}$ (AE: Ca, Sr) for symmetrical SOFC electrodes, Solid State Ionics 317 (2018) 194-200.

[12] Y. Guo, T. Guo, S. Zhou, Y. Wu, H. Chen, X. Ou, Y. Ling, Characterization of $Sr_2Fe_{1.5}Mo_{0.5}O_{6-\delta}$ - $Gd_{0.1}Ce_{0.9}O_{1.95}$ symmetrical electrode for reversible solid oxide cells, Ceram. Int. 45 (2019) 10969-10975.

[13] M.V. Sandoval, C. Cárdenas, E. Capoen, C. Pirovano, P. Roussel, G.H. Gauthier, Performance of $La_{0.5}Sr_{1.5}MnO_{4\pm\delta}$ Ruddlesden-Popper manganite as electrode material for symmetrical solid oxide fuel cells. Part A. The oxygen reduction reaction, Electrochim. Acta 304 (2019) 415-427.

[14] D.A. Osinkin, Kinetics of CO oxidation and redox cycling of $Sr_2Fe_{1.5}Mo_{0.5}O_{6-\delta}$ electrode for symmetrical solid state electrochemical devices, J. Power Sources 418 (2019) 17-23.

[15] H. Cai, L. Zhang, J. Xu, J. Huang, X. Wei, L. Wang, Z. Song, W. Long, Cobalte free $La_{0.5}Sr_{0.5}Fe_{0.9}Mo_{0.1}O_{3-\delta}$ electrode for symmetrical SOFC running on H_2 and CO fuels, Electrochim. Acta 320 (2019) 134642.

[16] O. Ben Mya, L. dos Santos-Gómez, J.M. Porras-Vázquez, M. Omari, J.R. Ramos-Barrado, D. Marrero-López, $La_{1-x}Sr_xFe_{0.7}Ni_{0.3}O_{3-\delta}$ as both cathode and anode materials for Solid Oxide Fuel Cells, Int. J. Hydrog. Energy 42 (2017) 23160-23169.

[17] S. Durán, N. Rangel, C. Silva, M.A. Macias, E. Capoen, C. Pirovano, A. Niemczyk, L. Suescun, P. Roussel, G.H. Gauthier, Study of $La_4BaCu_{5-x}Mn_xO_{13+\delta}$ materials as potential electrode for symmetrical-SOFC, Solid State Ionics 341 (2019) 115031.

[18] H. Iwahara, T. Esaka, T. Mangahara, Mixed conduction and oxygen permeation in the substituted oxides for $CaTiO_3$, J. Appl. Electrochem. 18 (1988) 173-177.

[19] J.C. Grenier, G. Schiffmacher, P. Caro, M. Pouchard, P. Hagenmuller, Etude par diffraction X et microscopie electronique du système $CaTiO_3-Ca_2Fe_2O_5$, J. Solid State Chem. 20 (1977) 365-379.

[20] J.C. Grenier, M. Pouchard, P. Hagenmuller, G. Schiffmacher and P. Caro, Ordre-désordre des lacunes anioniques dans les perovskites non stœchiométriques $CaTi_{1-2y}Fe_{2y}O_{3-y}$, J. Phys. Colloq. C7 38 (1977) C7-C84.

[21] D. Sutija, T. Norby, P.A. Osborg, P. Kofstad, AC van der Pauw measurements of the electrical conductivity of iron-doped calcium titanate, Electrochem. Soc. Proc. 93-4 (1993) 552-561.

[22] S. Marion, A.I. Becerro, T. Norby, Ionic and electronic conductivity in $CaTi_{1-x}Fe_xO_{3-\delta}$ (x=0.1–0.3), Ionics 5 (1999) 385-392.

[23] C.A. Mccammon, A.I. Becerro, F. Langenhorst, R.J. Angel, S. Marion, F. Seifert, Short-range ordering of oxygen vacancies in $CaFe_xTi_{1-x}O_{3-x/2}$ perovskites ($0 < \times < 0.4$), J. Phys. Condens. Matter 12 (2000) 2969-2984.

[24] F.M. Figueiredo, V.V. Kharton, J.C. Waerenborgh, A.P. Viskup, E.N. Naumovich, J.R. Frade, Influence of microstructure on the electrical properties of iron-substituted calcium titanate ceramics, J. Am. Ceram. Soc. 87 (2004) 2252-2261.

[25] L.A. Dunyushkina, A.V. Kuz'min, V.B. Balakireva, V.P. Gorelov, Electrical conduction nature and phase transition in $CaTi_{1-x}Fe_xO_{3-\delta}$ (x = 0.1–0.5), Russ. J. Electrochem. 42 (2006) 375-380.

[26] G.C. Mather, S. Islam, F.M. Figueiredo, Atomistic study of a CaTiO3-based mixed conductor: defects, nanoscale clusters, and oxide-ion migration, Adv. Funct. Mater. 17 (2007) 905-912.

[27] L.A. Dunyushkina, V.P. Gorbunov, High temperature electrical behaviour of $CaTi_{1-x}Fe_xO_{3-\delta}$ (x = 0–0.5) oxygen-ion, electronic and proton conductivity, Solid State Ionics 253 (2013) 169-174.

[28] C. Salles, J.M. Bassat J. Fouletier, D. Marinha, M.C. Steil, Oxygen pressure dependence of the ionic conductivity of iron-doped calcium titanate, Solid State Ionics 324 (2018) 103-108.

[29] C. Salles, M.C. Steil, J. Fouletier, M. Duttine, A. Wattiaux, D. Marinha, Long-term stability of iron-doped calcium titanate $CaTi_{0.9}Fe_{0.1}O_{3-\delta}$ oxygentransport membranes under non-reactive and reactive atmospheres, J. Membrane Sci. 583 (2019) 171-179.

[30] F.M. Figueiredo, J. Waerenborgh, V.V. Kharton, H. Näfe, J.R. Frade, On the relationships between structure, oxygen stoichiometry and ionic conductivity of $CaTi_{1-x}Fe_xO_{3-\delta}$ (x = 0.05, 0.20, 0.40, 0.60), Solid State Ionics 156 (2003) 371-381.

[31] J.M. Porras-Vázquez, P.R. Slater, Synthesis and Characterization of Oxyanion-Doped Cobalt Containing Perovskites, Fuel Cells 12 (2012) 1056-1063.

[32] C.A. Hancock, J.M. Porras-Vázquez, P.J. Keenan, P.R. Slater, Oxyanions in perovskites: from superconductors to solid oxide fuel cells, Dalton Trans. 44 (2015) 10559-10569.

[33] A. Jarvis, P.R. Slater, Investigation into the effect of sulfate and borate incorporation on the structure and properties of $SrFeO_{3-\delta}$, Crystals 7 (2017) 169.

[34] A.D. Smith, M.S. James, P.R. Slater, Effect of Si-doping on the structure and conductivity of $(Sr/Ca)_2MnFeO_{6-\delta}$ systems, ECS Trans. 91 (2019) 1425-1436.

[35] J.M. Porras-Vázquez, T.F. Kemp, J.V. Hanna, P.R. Slater, Synthesis and characterization of oxyanion-doped manganites for potential application as SOFC cathodes, J. Mater. Chem. 22 (2012) 8287-8293.

[36] J.M. Porras-Vázquez, P.R. Slater, Synthesis of oxyanion-doped barium strontium cobalt ferrites: Stabilization of the cubic perovskite and enhancement in conductivity, J. Power Sources 209 (2012) 180-183.

[37] J.M. Porras-Vázquez, T. Pike, C.A. Hancock, J.F. Marco, F.J. Berry, P.R. Slater, Investigation into the effect of Si doping on the performance of $SrFeO_{3-\delta}$ SOFC electrode materials, J. Mater. Chem. A 1 (2013) 11834-11841.

[38] Z. Wang, C. Jin, J. Sui, C. Li, R. Yang, Phosphorus-doped $SrCo_{0.5}Mo_{0.5}O_3$ perovskites with enhanced bifunctional oxygen catalytic activities, Int. J. Hydrog. Energy 43 (2018) 20727-20733.

[39] Z. Li, L. Lv, J. Wang, X. Ao, Y. Ruan, D. Zha, G. Hong, Q.H. Wu, Y. Lan, C.D. Wang, J. Jiang, M. Liu, Engineering phosphorus-doped $LaFeO_3$- perovskite oxide as robust bifunctional oxygen electrocatalysts in alkaline solutions, Nano Energy 47 (2018) 199-209.

[40] Y. Zhu, W. Zhou, J. Sunarso, Y. Zhong, Z. Shao, Phosphorus-doped perovskite oxide as highly efficient water oxidation electrocatalyst in alkaline solution, Adv. Funct. Mater. 26 (2016) 5862-5872.

[41] L. dos Santos-Gómez, J.M. Compana, S. Bruque, E.R. Losilla, D. Marrero-López, Symmetric electrodes for solid oxide fuel cells based on Zr-doped $SrFeO_{3-\delta}$, J. Power Sources 279 (2015) 419-427.

[42] PANalytical X′Pert HighScore Plus Suite, B. V., Lelyweg 1, 7602 EA Almelo, The Netherlands, 2014.

[43] A.C. Larson, R.B. von Dreele, General Structure Analysis System (GSAS); Los Alamos National Laboratory, 1994.

[44] J.C.C. Abrantes, Estereologiá software, Polytechnic Institute of Viana do Castelo, Viana do Castelo, Portugal, 1998.

[45] A.I. Becerro, F. Langenhorst, R.J. Angel, S. Marion, C.A. McCammon, F. Seifert, The transition from short-range to long-range ordering of oxygen vacancies in $CaFe_xTi_{1-x}O_{3-x/2}$ perovskites, Phys. Chem. Chem. Phys. 2 (2000) 3933-3941.

[46] J.C. Waerenborgh, F.M. Figueiredo, J.R. Frade, M.T. Colomer, J.R. Jurado, Fe^{4+} content and ordering of anion vacancies in partially reduced $AFe_xTi_{1-x}O_{3-y}$ (A = Ca, Sr; x≤0.6) perovskites. An ^{57}Fe Mössbauer spectroscopy study, J. Phys.: Condens. Matter 13 (2001) 8171-8187.

[47] V.V Kharton, F.M. Figueiredo, A.V. Kovalevsky, A.P. Viskup, E.N. Naumovich, J.R. Jurado, J.R. Frade, The oxygen diffusion in, and thermal expansion of, $SrTiO_{3-\delta}$ and $CaTiO_{3-\delta}$ based materials, Defect Diffusion Forum 186/187 (2000) 119-136.

[48] L. dos Santos-Gómez, J.M. Porras-Vázquez, E.R. Losilla, D. Marrero-López, Ti-doped $SrFeO_3$ nanostructured electrodes for symmetric solid oxide fuel cells, RSC Adv. 5 (2015) 107889-107895.

[49] L. dos Santos-Gómez, J.M. Porras-Vázquez, E.R. Losilla, D. Marrero-López, Improving the efficiency of layered perovskite cathodes by microstructural optimization, J. Mater. Chem. A 5 (2017) 7896-7904.

[50] J. Canales-Vázquez, J.C. Ruíz-Morales, D. Marrero-López, J. Pena-Martínez, P. Núñez, P. Gómez-Romero, Fe-substituted $(La,Sr)TiO_3$ as potential electrodes for symmetrical fuel cells (SFCs), J. Power Sources 171 (2007) 552-557.

[51] B. Lin, S. Wang, X. Liu, G. Meng, Simple solid oxide fuel cells, J. Alloys Compd. 490 (2010) 214-222.

Table 1. Cell parameters and normalized cell volumes for $CaTi_{0.6-x}Fe_{0.4}P_xO_{3-\delta}$ series (x = 0-0.075) in air and $5\%H_2$-Ar obtained from XRPD data analysis.

		P_0	$P_{0.025}$	$P_{0.05}$	$P_{0.075}$
Air	**a (Å)**	3.8321(1)	3.8287(1)	3.8277(1)	3.8271(1)
	V/Z(Å^3)	56.27(1)	56.13(1)	56.08(1)	56.05(1)
	R$_{WP}$(%)	3.82	2.45	2.60	2.67
	R$_F$(%)	4.79	4.42	4.45	4.76
	Ca$_{10}$(PO$_4$)$_6$(OH)$_2$(%)	-	-	2.4	4.0
5%H$_2$-Ar	**a (Å)**	5.4225(3)	3.8359(1)	3.8362(1)	3.8364(1)
	b (Å)	5.4576(3)	-	-	-
	c (Å)	7.6702(3)	-	-	-
	V/Z(Å^3)	56.75(3)	56.44(1)	56.45(1)	56.46(1)
	R$_{WP}$(%)	3.31	3.22	2.93	2.97
	R$_F$(%)	5.12	8.05	7.70	7.98

Figure captions

Figure 1. XRPD patterns for $CaTi_{0.6-x}Fe_{0.4}P_xO_{3-\delta}$ series (a) x = 0 and (b) x =0.025 sintered in the temperature range between 800 and 1400 ºC for 4 h.

Figure 2. XRPD patterns for $CaTi_{0.6-x}Fe_{0.4}P_xO_{3-\delta}$ series (x = 0, 0.025, 0.05 and 0.075) (a) sintered at 1400 and 1200 ºC for undoped and P-doped compounds, respectively, for 4 h and (b) calcined at 800 ºC for 48 h under $5\%H_2$-Ar.

Figure 3. Oxygen deficiency and average oxidation state of iron as a function of P-content, $CaTi_{0.6-x}Fe_{0.4}P_xO_{3-\delta}$ (x= 0-0.075).

Figure 4. SEM and EDS image of surface of $CaTi_{0.6-x}Fe_{0.4}P_xO_{3-\delta}$ series (x = 0, 0.025 and 0.05) compounds.

Figure 5. XRPD patterns for $P_{0.025}$/YSZ mixture (1:1 wt.%) at room temperature and after firing between 800 and 1000 ºC in air.

Figure 6. Arrhenius plots of $CaTi_{0.6-x}Fe_{0.4}P_xO_{3-\delta}$ (x= 0-0.075) in (a) air and (b) $5\%H_2$-Ar. (c) R_p values of P_0 and $P_{0.025}$ in air and $5\%H_2$-Ar

Figure 7. (a) Current-voltage and power density curves of $P_{0.025}$/YSZ/$P_{0.025}$ symmetrical cell and (b) SEM image of the cross-section of the cell.

Supplementary figure captions

Figure S1. Rietveld plot of $CaTi_{0.575}Fe_{0.4}P_{0.025}O_{3-\delta}$ heated at 1200 ºC for 4 h.